

# Attribution of aerosol particle number size distributions to major sources using a 11-year-long urban dataset

Máté Vörösmarty<sup>1</sup>, Philip K. Hopke<sup>2,3</sup>, and Imre Salma<sup>4</sup>

<sup>1</sup> Hevesy György Ph.D. School of Chemistry, Eötvös Loránd University, Budapest, Hungary

<sup>2</sup> Department of Public Health Sciences, University of Rochester School of Medicine and Dentistry, Rochester, NY, USA

<sup>3</sup> Institute for a Sustainable Environment, Clarkson University, Potsdam, NY, USA

<sup>4</sup> Institute of Chemistry, Eötvös Loránd University, Budapest, Hungary

**Correspondence:** Imre Salma (salma.imre@ttk.elte.hu) and Máté Vörösmarty (vmate6@student.elte.hu)

**Abstract.** Source apportionment was performed using size-segregated atmospheric particle number concentrations (PNCs) in 27 size channels over a diameter range of 6–1000 nm augmented by air pollutants ~~all~~ with a time resolution of 1 h in ~~the urban background of~~ Budapest for 11 full years ~~in separate seasons~~. The input dataset was ~~corrected~~ treated for the effect of the local meteorology by dispersion ~~correction~~ dispersion normalisation using the ventilation coefficient defined as the planetary boundary mixing layer height multiplied by the wind speed. Both the uncorrected and ~~dispersion-corrected~~ datasets were evaluated using positive matrix factorization in separate seasons. Six source types including nucleation, two road vehicle emission sources separated into a semi-volatile fraction and a solid core fraction, diffuse urban source, secondary inorganic aerosol (SIA), and ozone-associated secondary aerosol were identified, characterised and quantified. ~~The ventilation correction substantially modified the input concentrations, while the differences in the corrected to uncorrected ratios for the contributions remained within 5 %.~~ The dispersion correction did not considerably change the profiles and diel variations or patterns of the sources, while it substantially modified the relative shares of the nucleation source in all seasons. The ~~overall~~ mean relative contributions of the traffic emission ~~sources was (of 60 %) point that on-road motor vehicles were the leading source of particle numbers. They did not show considerable seasonal variability.~~ The nucleation was responsible for ~~20–24~~ 20–24 % of the PNC annually as a lower estimate. It exhibited a compound character consisting of photochemically induced nucleation and traffic-related nucleation. ~~The former process occurs on regional or urban spatial scales around noon, whereas the latter process happens when the gas phase vapours in the vehicle exhaust cool, and the resulted supersaturated vapours nucleate outside the source.~~ Its contributions were the highest in spring ~~(somewhat smaller in summer and autumn)~~ and the lowest in winter. The ~~contributions shares from of the SIA and~~ the urban diffuse and the SIA source types were the largest in autumn and winter, and in spring and summer ~~approximately 10 % in spring, summer, and 12 %–15 % in autumn and winter, respectively, but they were typically  $< \approx 10$  %.~~ The O<sub>3</sub>-associated secondary aerosol made up the smallest (~~6–~~  $< \approx 3$  %)

34 ~~contributions~~portion of particles on an annual basis. Directionality variations investigated byThe  
35 conditional bivariate probability function analysis ~~were used to locate the likely source areas, and~~ showed  
36 considerable spatial variations in the source origin. The combination of the size-segregated particle  
37 number concentrations, wide overall range of the size channels, considerably long dataset, dispersion  
38 correction and modelling over separate seasons jointly lead to a unique adaptation of the source  
39 apportionment, and yielded novel and valuable insights into the urban aerosol sources and processes both  
40 for Budapest and in general.

## 41 **1 Introduction and objectives**

42 Particulate matter (PM) plays a vital role in the urban air quality worldwide. It is often quantified by the  
43 mass of particles, which ~~is established as~~ belongs to the group of the ~~key~~Key Pollutants or ~~criteria~~  
44 Criteria Aair ~~pollutant~~ Pollutants (EU EEA, 2023; US EPA, 2023). Coarse- and accumulation-mode  
45 particles make up most PM mass, whereas the mass contribution of the ultrafine (UF) particles  
46 (traditionally defined with  $d < 100$  nm) is negligible (e.g., Salma et al., 2002). Despite the fact that UF  
47 particles make up  $> 80$  % of total particle numbers in cities (Trechera et al., 2023). At relatively low PM  
48 mass and high UF particle concentrations, it is the particle number that represents the potential danger to  
49 human health better than the PM mass. There are toxicological (Oberdörster et al., 2005; HEI Review  
50 Panel, 2013), clinical (Chalupa et al., 2004) and epidemiological (Kreyling et al., 2006; Wang, M. et al.,  
51 2019) studies, which suggest that the UF particles can cause adverse health effects. Inhalation of very  
52 small insoluble particles can lead to excess health risk relative to the effects of the coarse or fine particles  
53 having similar chemical composition (Oberdörster et al., 2005; HEI Review Panel, 2013).~~Inhalation of~~  
54 ~~very small insoluble particles can particularly lead to excess health risk relative to coarse or fine particles~~  
55 ~~of the similar chemical composition (Oberdörster et al., 2005; HEI Review Panel, 2013).~~ This threat is  
56 caused by the vast number of the deposited particles in the respiratory system, their relatively large total  
57 surface area and small size (Oberdörster et al., 2005; Braakhuis et al., 2014; Salma et al., 2015; Riediker  
58 et al., 2019). The World Health Organization identified the UF particles as a potential risk factor for  
59 humans (WHO, 2021).

60

61 Particle number size distribution (PNSD) is a basic property of the aerosol system. It can vary  
62 considerably over space and time. Formation and atmospheric transformation processes essentially  
63 contribute to this variability. Apart from the vicinity of intensive sources of UF particles, the PNSDs  
64 change rates become much slower. Under these more balanced conditions, the PNSDs can be separated  
65 into such size modes that are associated with source types or aggregate sources (Hopke et al. 2022 and

66 references therein). The PNSDs in the ambient air usually consist of nucleation, Aitken and accumulation  
67 modes. The nucleation mode can be associated with regional atmospheric new aerosol particle formation  
68 (NPF) and growth events (Kulmala et al., 2003), and local or sublocal nucleation connected with  
69 combustion sources such as internal combustion engines (Kittelson et al., 2022 and references therein),  
70 residential heating and food cooking with natural gas (Li and Hopke, 1993). The Aitken-mode particles  
71 are usually emitted into the air and can contain largely variable portions of semi-volatile components  
72 condensed on solid core (Morawska et al., 2008; Harrison et al., 2019; Rönkkö and Timonen, 2019;  
73 Kittelson et al., 2022). The accumulation-mode particles ordinarily result from transformation processes  
74 such as condensation growth, physical and chemical ageing or water activation processes of Aitken-mode  
75 or nucleated particles. The naming, modal diameters and attribution of the modes to the specific formation  
76 processes for some concrete specific sources such as mobile vehicles (which can make up the major part  
77 of particle numbers in cities) can largely vary in the literature (Kittelson et al., 2022).

78

79 Primary pollutants (together with the particle number size distributions of primary particles)Primary  
80 pollutants (including particle number concentrations and size distributions) can be also affected by  
81 meteorological processes such as atmospheric mixing and transport due to their dispersion (dilution or  
82 enrichment). The dispersion is often governed by solar radiation through planetary boundary mixing layer  
83 height (MLH), wind or precipitation (Andronache, 2004; Kumar et al., 2011). These conditions can  
84 substantially affect both larger orographic basins and smaller valleys (Leahey, 1972; Salma et al., 2020).  
85 The dispersion of primary particles is essentially related to the available air volume in which they are  
86 mixed (Holzworth, 1967; Ashrati et al., 2009). In cities, this volume is determined by the MLH and wind  
87 speed (WS) in the first approach. It is noted that meteorological variables may affect secondary pollutants  
88 and particles in a more complex way with respect to the primary pollutants and particles.

89

90 The shape of PNSDs is influenced by the formation and transformation processes of particles, and by  
91 meteorological conditions (Li et al., 2023).~~The spatial and temporal diversity and dynamics of the~~  
92 ~~formation and transformation processes, and of meteorological conditions are reflected in the PNSDs as~~  
93 ~~far as both their integrated concentration and shape are concerned (Li et al., 2023).~~ Thus, size distributions  
94 can be used for identifying and quantifying various source types. These sources basically differ from  
95 those dominating the PM mass. The particle number concentrations are nonconservative compared to the  
96 PM mass. Attribution of PNSDs to different source types and their quantification are desirable and  
97 essential since many basic properties, atmospheric behaviour of particles as well as their health,  
98 environmental and climate effects depend on their number (and not on their mass) concentration (e.g.,  
99 Ibaldo-Mulli et al., 2002; Meng et al., 2013; Corsini et al., 2019). Source apportionment can also yield

100 valuable knowledge for creating air quality regulatory strategies for particle numbers or their source  
101 specific exposure metrics. Therefore, there is recently a considerable and increasing scientific interest in  
102 source apportionment studies on PNSDs (Beddows et al., 2019; Dai et al., 2021; Hopke et al., 2022;  
103 Teinilä et al., 2022; Conte et al., 2023; Crova et al., 2024; Rowell et al., 2024). Studies based on multiple-  
104 year-long data are still scarce (de Jesus et al., 2020).

105

106 Source apportionments can be achieved by multivariate modelling (Hopke, 1991). Positive matrix  
107 factorisation (PMF; Paatero and Tapper, 1993, 1994) is one of the most widely used, well established and  
108 efficient technique for this (Hopke, 2016; Hopke et al., 2020). The PMF modelling was successfully  
109 applied to mass concentrations of aerosol constituents and gases (e.g., Viana et al., 2008; US EPA, 2014;  
110 [Belis et al., 2020](#)). The main differences between the PMF deployed on particle number size distribution  
111 data with respect to that on mass concentrations include different attitudes to handling zero data and  
112 values below the detection limits, and to estimating the observation uncertainties (Ogulei et al., 2007).

113

114 To study the phenomenon of the urban atmospheric NPF and growth in Budapest, PNSDs in a diameter  
115 range of 6–1000 nm, meteorological properties and air pollutants were measured for 11 full measurement  
116 years. They belong to the longest critically evaluated urban datasets of this kind in the world. Utilising  
117 this readily available dataset for source apportionment by PMF method offers different and  
118 comprehensive insights into the sources of particle numbers. Such long-term observations are particularly  
119 valuable as they can statistically reveal information which were hidden in the noise on shorter time scales  
120 (Kulmala et al., 2023). The main objectives of this study are 1) to present and discuss the results and  
121 experience gained from the source apportionment of PNSDs by applying the PMF method for separate  
122 seasons in Budapest; 2) to quantify the effect and importance of the [atmospheric](#) dispersion correction; 3)  
123 to interpret the main sources and their spatial distributions; and 4) to determine the relevance of the  
124 sources. [The combined application of the size segregated–particle number concentrations, wide range of  
125 the size channels, considerably long dataset, dispersion correction and modelling over separate seasons  
126 can lead to novel insights into the aerosol sources, transformation and transport processes of particle  
127 numbers in cities.](#) Our conclusions can also contribute ~~to the general understanding of the sources,  
128 transformation and transport processes of particle numbers in cities and~~ to developing [novel-innovative](#)  
129 air quality regulatory policy for the particle numbers.

## 130 2 Methods

### 131 2.1 Experimental part and data treatment

132 The measurements were performed at two urban sites in Budapest. Most of them were conducted at the  
133 Budapest platform for Aerosol Research and Training (BpART) Laboratory (47°28'29.9" N, 19°3'44.6"  
134 E; 115 m above mean sea level, m.s.l.) of the Eötvös Loránd University (Salma et al., 2016a). The  
135 measurement site is located 85 m from the River Danube, which flows through the city centre. The  
136 location represents an urban background site due to its geographical and meteorological conditions. The  
137 other measurement site was in a wooden area of the Konkoly Astronomical Observatory (47°30'00" N,  
138 18°57'47" E; 478 m above m.s.l.) at the NW border of the city. Since the prevailing wind direction in the  
139 area is NW, the latter site represents the near-city background. The exact timings of the measurement  
140 years are detailed in Table S1 in the Supplement. The experimental data from the two measurement sites  
141 were merged into one dataset which was evaluated jointly.

142  
143 The PNSDs were measured using a flow-switching-type differential mobility particle sizer system, which  
144 operates in an electrical mobility diameter range from 6 to 1000 nm in the dry state of particles (relative  
145 humidity, RH < 30 %) separating the particles into 27 size channels with a time resolution of  $\tau = 8$  min  
146 (Salma et al., 2011, 2016b, 2021). The nominal diameters of the 27 channels are 6.0, 7.3, 8.9, 10.8, 13.2,  
147 16.0, 19.5, 23.7, 28.9, 35.2, 42.9, 52.1, 63.4, 77.2, 93.9, 114, 139, 169, 206, 250, 304, 371, 451, 550, 670,  
148 816, and 994 nm. This list facilitates the exact interpretation of the factor profiles in Figs. 2a–4a and  
149 ~~S5aS10a–S7aS12a~~. The concentrations of NO, NO<sub>x</sub>/NO<sub>2</sub>, CO, O<sub>3</sub>, SO<sub>2</sub>, PM<sub>10</sub> mass were acquired from  
150 the closest measurement stations of the National Air Quality Network located 4.5 km from the urban  
151 background site and 6.9 km from the near-city background site in the upwind prevailing direction (Salma  
152 et al., 2020). The time resolution of these measurements was 1 h. Air temperature ( $T$ ), RH, ~~wind speed~~  
153 ~~(WS)~~, wind direction (WD) and global radiation were measured at the BpART Laboratory and above the  
154 rooftop level of the building complex (at a height of 45 m above the nearest street). The wind data above  
155 the rooftop level were utilised in the present study and were recorded by standardized sensors (WAA15A  
156 and WAV15A, both Vaisala, Finland) with  $\tau = 10$  min. Mixing layer height data ( $\tau = 1$  h) were extracted  
157 from the Copernicus Climate Change Service (ERA5 Family datasets, ECMWF reanalysis; Hersbach et  
158 al., 2023).

159  
160 The data were expressed in local time (UTC+1 or daylight-saving time UTC+2). This was chosen since  
161 the activities of the inhabitants greatly influence the atmospheric concentrations and size distributions in  
162 cities (Mikkonen et al., 2020). Hourly mean PNSDs were derived from the experimental data to reduce

163 their fluctuations and the number of the missing data. Atmospheric concentrations in each size channel  
164 and of the total particle number concentrations ( $N_{6-1000}$ ) were calculated and further evaluated. The  
165 investigated time interval involved 11 full measurement years (Table S1). The data from the two urban  
166 sites were joined and evaluated together. The residuals and the goodness of the fits in the PMF modelling  
167 did not indicate significant differences between the respective factor profiles in the urban background and  
168 near-city background. Additionally, this multi-site approach is expected to improve the efficiency of the  
169 source apportionment (Pandolfi et al., 2010; Dai et al., 2020; Harni et al., 2023). The median  $N_{6-1000}$  and  
170 atmospheric concentrations of pollutants over the measurement years are also summarised in Table S1.

171

172 The overall dataset was finally split into separate subsets for meteorological seasons (March, April, May  
173 as spring, June, July, August as summer, September, October, November as autumn and December,  
174 January, February as winter) to fulfil one of the basic requirements of the PMF method on the consistency  
175 of the source profile over the time interval considered (Zhou et al., 2004; Ogulei et al., 2007). The PMF  
176 modelling was performed separately on each season joined over all 11 years. The missing concentration  
177 values in the input dataset were replaced by the medians with 3-times the measurement uncertainty of the  
178 seasonal dataset. The data coverage for the input data was typically > 85 %. The total number of  
179 observations for the PNSDs are shown in Fig. S2S6. The seasonal means and standard deviations (SDs)  
180 of the meteorological properties are summarised in Table S2.

## 181 2.2 Source apportionment modelling

182 The source apportionment was performed using the PMF method with the equation solver Multilinear  
183 Engine 2 (ME-2); ~~as described by Paatero, 1999;~~ Hopke et al. (2023). The method decomposes the input  
184 dataset into a factor (source) profile matrix and a factor contribution matrix with a user-specified factor  
185 number based on the covariances between the variables. The PMF iteratively optimizes the objective  
186 parameter  $Q$ , which is calculated on the individual residuals ( $e$ ) and the uncertainties ( $s$ ) for the  
187 observation  $i$  and variable  $j$ :

$$188 \quad Q = \sum_{i=1}^m \sum_{j=1}^n \left( \frac{e_{ij}}{s_{ij}} \right)^2, \quad (1)$$

189 where  $m$  and  $n$  are the maximum number of observations and variables, respectively.  $Q_{true}$  was calculated  
190 with all data points, whereas  $Q_{robust}$  was determined excluding the poorly fitted data points (i.e. when their  
191 uncertainty-scaled residuals were > 4). The uncertainties of the particle number concentrations in a size  
192 channel  $j$  were estimating as (Ogulei et al., 2007):

$$193 \quad \sigma_{ij} = (A \times \alpha) \times (N_{ij} + \bar{N}_j), \quad (2)$$



194 
$$s_{ij} = \sigma_{ij} + C_3 \times N_{ij}, \quad (3)$$

195 where  $\sigma$  is the estimated individual measurement uncertainty for an observation,  $N$  represents the observed  
 196 concentration,  $\bar{N}$  is the arithmetic mean of the observed concentrations in the respective variable,  $\alpha$  is  
 197 constant (of 0.01), which value is fine-tuned by  $A$  around its nominal value,  $s$  is the overall uncertainty  
 198 matrix, and  $C_3$  is constant (0.1 for size channels, 0.2 for  $N_{6-1000}$  and 0.15 for air pollutants), which is also  
 199 tuned. Specifying too low uncertainties relative to the true error level results in overweighting those  
 200 datapoints, while larger uncertainties yields downweighting (Hopke, 2020). Assigning Moderate  
 201 moderately lower statistical weights~~downweighting~~ exerts less sensitive effect on the modelling results  
 202 than overweighting, and the overdetermined uncertainties can also obscure the concentration data. These  
 203 selections ~~and relationships~~ are widely accepted in the PNSD source apportionment studies (Hopke et al.  
 204 2020 and references therein).

205

206 The addition of the air pollutants is beneficial for the PMF as the new quantities provide insights into the  
 207 sources or atmospheric processes that produce the measured size distributions, and reduce the rotational  
 208 ambiguity of the model by complementing the edge points (Paatero, 1999; Hopke, 2016).

209

210 Dispersion of the atmospheric concentrations due to the changes of meteorological conditions can result  
 211 in additional covariance. This effect can be corrected ~~for~~ by dispersion normalization of the input dataset  
 212 with the ventilation coefficient (VC; Ashrati et al., 2009). In this approach, the available air volume for  
 213 the atmospheric dispersion is proportional to the product of the  $MLH_i$  and the vectorial mean of the wind  
 214 speed ( $u_i$ ) for the observation  $i$ :

215 
$$VC_i = MLH_i \times u_i. \quad (4)$$

216 The hourly mean  $u_i$  values were obtained from the 10-min WS and WD data using vectorial averaging.  
 217 The occurrence of the zero hourly-mean  $u_i$  value was very low in the resulted dataset; the share of  $u_i <$   
 218 0.1 m s<sup>-1</sup> was 0.06 %. The concentration data ( $C_i$ ) were multiplied by the ratio (called ventilation  
 219 coefficient ratio,  $VC_{ratio}$ ) of the corresponding  $VC_i$  and its ~~seasonal-overall~~ mean value  $\overline{VC}$  (~~called~~  
 220 ~~ventilation coefficient ratio~~):

221 
$$C_{Vi} = C_i \times \frac{VC_i}{\overline{VC}}. \quad (5)$$

222 The ventilation coefficient represents the maximum volume into which the particles undergo dilution after  
 223 their release into or formation within the ambient air per unit time (Dai et al., 2021). The main purpose  
 224 of this treatment is to correct each concentration data to have the same ventilation coefficient as the mean  
 225 VC over the whole, 11-year-long dataset. The latter quantity was 1768 m<sup>2</sup> s<sup>-1</sup> in our case.

226

227 After completing the PMF analysis on the corrected dataset, the derived source contributions were divided  
228 by the respective VC ratios to obtain the real contributions. The source apportionment modelling was  
229 performed independently both on the uncorrected and dispersion-corrected concentrations. The results  
230 derived from the uncorrected dataset (i.e.,  $C_i$  concentrations) are referred as uncorrected PMF data, while  
231 those obtained from the corrected dataset ( $C_{vi}$  concentrations) are denoted as dispersion-corrected (DC-)  
232 PMF data.

233

234 The PMF solutions were explored in 50 runs with different configurations for each dataset. The factor  
235 count was changed between 4 to 12; the uncertainty parameters were modified from 0.01 to 0.05 for ( $\alpha \times$   
236  $A$ ), and between 0.01 and 0.5 for  $C_3$ . Increased uncertainty settings were adopted for the smallest ( $< 10$   
237 nm) and the largest ( $> 800$  nm) size channels since their uncertainties were proven to be larger  
238 (Wiedensohler et al., 2012), and for the air pollutants since they were set as weak variables. The final  
239 solution was reached through a trial-and-error approach. The final parameters of the uncertainty  
240 estimations of the input data are summarised in Table S3. Additional uncertainty estimations were run  
241 using bootstrap and displacement analyses. Some summary results of this evaluation are shown in Figs.  
242 S1–S4 for the factors (identified later as source types) and seasons. These auxiliary calculations and the  
243 comparison of their outcomes also mark and confirm that the final selection of the modelling parameters  
244 and input uncertainty data were reasonable and appropriate.

245

246 From the analysis point of view, the best solution (approved later as the final solution) was chosen to  
247 meet the criteria that the convergence is achieved in the robust manner; its  $Q_{true}$  and  $Q_{robust}$  diagnostic  
248 values are among the lowest values; the scaled residuals are distributed preferably normally between  $-3$   
249 and  $+3$ ; and that the goodness of the fit (expressed by the coefficient of determination,  $r^2$ ) for the strong  
250 variables are typically  $> 0.85$ . From the interpretation aspect, the main requirements were that the solution  
251 is physically interpretable based on the size profiles, shows sensible diel patterns, weekly and annual  
252 tendencies, and is acceptable as far as directional probability function plots are concerned.

253

254 Spatial variations of the source intensities and other properties were derived by conditional bivariate  
255 probability function (*polarPlot()*) of the ‘openair’ package (Carlsaw and Ropkins, 2012; Uria-Tellaexte  
256 and Carlsaw, 2014). The method utilizes WS and WD data to create plots of directionality. The plots  
257 derived from the uncorrected and corrected PMF modelling were compared using the *polarDiff()* function



258 of the package. Further statistical evaluations and presentations were accomplished by a laboratory-  
259 developed application AeroSoLutions2 in conjunction with the Accord.NET Framework (Souza, 2014).

## 260 3 Results and discussion

### 261 3.1 Effects of the dDispersion correction ~~and its effect~~ on the input dataset

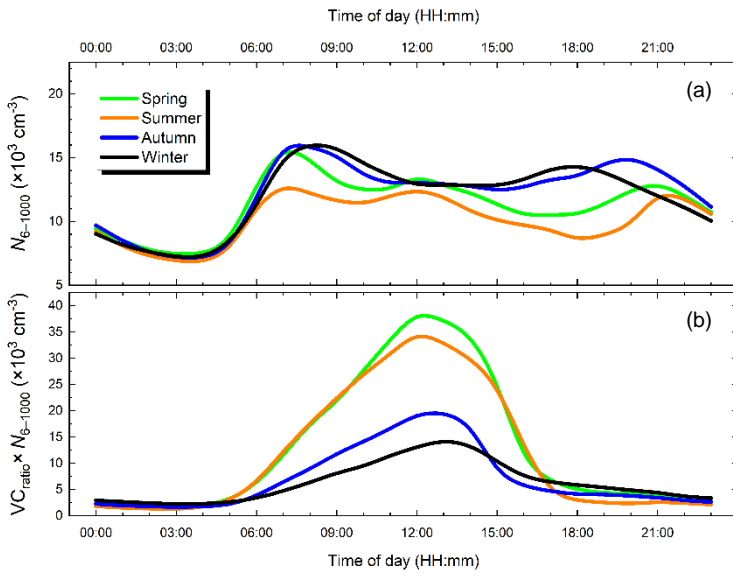
262 The mean diel variations of the ventilation coefficient ratio and of its MLH and WS constituents are  
263 shown in Fig. ~~S1-S5~~ and discussed in the Supplement. The effects of the dispersion correction on the PMF  
264 input data are demonstrated by the diel variations of the uncorrected and dispersion-corrected  $N_{6-1000}$  for  
265 separate seasons (Fig. 1). The structure of the uncorrected curves (Fig. 1a) was discussed and explained  
266 earlier (Salma et al., 2011, 2020; Thén and Salma, 2021). Conclusively, there are three peaks present with  
267 variable relative areas in the diel variations; namely an early-morning peak and an evening peak at the  
268 rush hours of 06:00–08:00 and 18:00–21:00, respectively, largely generated by road vehicle traffic, and  
269 a midday peak predominantly produced by NPF events driven by photochemistry.~~In summary, they show~~  
270 ~~three peaks; early morning and evening peaks at the rush hours of 06:00–08:00 and 18:00–21:00,~~  
271 ~~respectively, largely generated by vehicular road traffic, and a midday peak primarily produced by NPF~~  
272 ~~events driven by photochemistry.~~ The curve in summer seems to be below the other lines during the  
273 daylight period. The concentrations monotonically decreased from 23:00 to 05:00 and were virtually  
274 identical to each other.

275

276 The extent and shape of the diel curves of the atmospheric concentrations multiplied by the ventilation  
277 ratio were vastly different from the uncorrected lines (Fig. 1b). They all consisted of a broad, single,  
278 structured peak. The largest maxima of the peaks were observed in spring and summer, while the peaks  
279 in autumn and winter were considerably lower. The shift in the timing of the maxima was influenced by  
280 the clock change for the daylight-saving periods. The curves exhibited monotonically decreasing  
281 tendency in evening and reached a constant level during the night. ~~These results emphasize that the input~~  
282 ~~data for the PMF modelling became different after the dispersion correction from the uncorrected dataset.~~

283

284  
285  
286  
287  
288  
289  
290  
291  
292  
293  
294  
295  
296  
297



298 **Figure 1.** The mean diel variation of the uncorrected ( $N_{6-1000}$ ; a) and dispersion-corrected total particle number concentrations  
299 ( $VC_{ratio} \times N_{6-1000}$ ; b) separately for spring, summer, autumn and winter.

### 300 3.2 Interpretation of the factors

301 The regression lines of the measured and uncorrected modelled  $N_{6-1000}$  are shown in Fig. S2S6. The curves  
302 and their statistics indicate that the PMF modelling yielded reasonable agreement with the experimental  
303 data. Based on the selection criteria described in Sect. 2.2, six-factor solutions were accepted for both the  
304 uncorrected and dispersion-corrected datasets in each season. More factors resulted in unreasonable  
305 splitting of some factors (even in winter), whereas a smaller number of factors yielded questionable  
306 merging the factors. The approved final solutions represent physically sensible approximation for  
307 Budapest. The PMF results derived from the uncorrected input data are interpreted in Sects. 3.2.1–3.2.5.  
308 The related plots for the 3 major sources are displayed in the article (Figs. 2–4), whereas those for the  
309 remaining 3 sources are shown in the Supplement (Figs. S10–S12) to communicate our primary messages  
310 in a focused manner. The directionality plots of the sources for the uncorrected PMF results for separate  
311 sources modelling are presented in Fig. S9–S19.

#### 312 3.2.1 Nucleation

313 The factor associated with the smallest particles in our experimental setup was characterised by a single  
314 mode in the source profile with a diameter range from 6 to 25 nm (Fig. 2a). This range ordinarily  
315 represents the nucleation mode in NPF studies (Kerminen et al., 2018) and corresponds to its typical time-  
316 averaged evolution (e.g., Salma and Németh, 2019). The contributions of the factor to the concentrations  
317 were the largest in spring and the smallest in winter (Fig. 2b). This property coincides with the relative  
318 occurrence frequency of the NPF events in the Budapest area (the Carpathian Basin; Salma et al., 2016b,

319 2021). The diel variations for the  $N_{6-1000}$  of this factor showed the highest intensity at 12:00 in all seasons  
 320 with the largest peak in spring and with the smallest peak (if any) in winter (Fig. 2c).

321

322

323

324

325

326

327

328

329

330

331

332

333

334

335

336

337

338

339

340

341

342

343

344

345

346

347

348

349

350

351

352

353

354

355

356

357

358

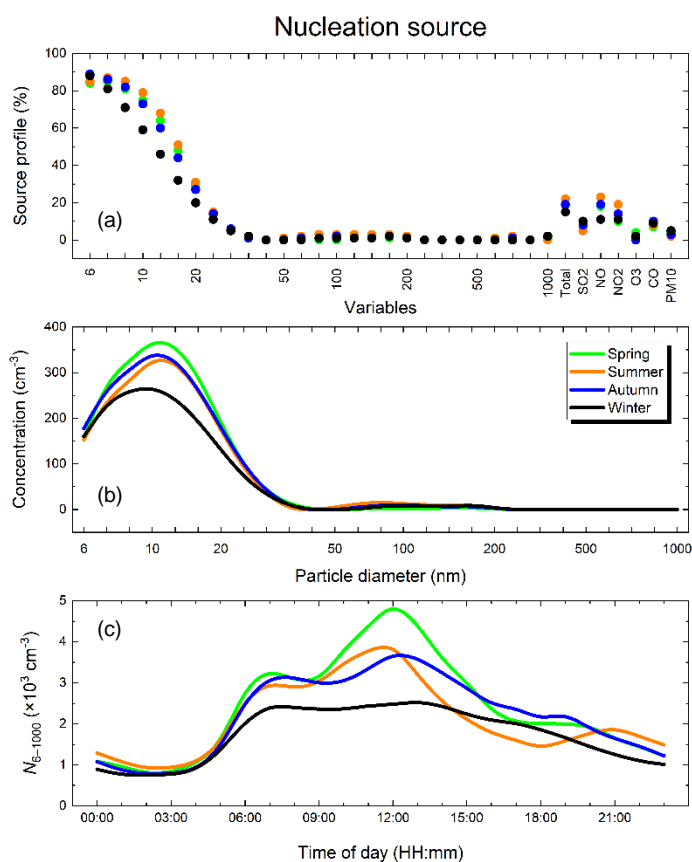


**Figure 2.** Relative factor profile (a), factor contribution to the particle number concentrations in the size channels (b), and the mean diel variation of the total particle number concentrations ( $N_{6-1000}$ ; c) assigned to the compound nucleation source in the uncorrected PMF modelling for spring, summer, autumn and winter. The exact diameters of the size channels are listed in Sect. 2.1.

The time series unambiguously indicated additional peaks in the early-morning and evening rush hours in addition to the midday peak (Figs. 2c and S3aS7a, b). The factor also exhibited non-negligible association with NO, NO<sub>2</sub> and CO with varying degrees (Fig. 2a). These results suggest that there is connection between this factor and the road vehicle traffic, particularly in non-winter seasons. The compound character of the factor was recognised earlier (Rivas et al., 2020). In our results, the importance of the traffic-related subfactor was higher on weekdays compared to weekends (particularly in the early-morning rush hours on Sunday) when the traffic intensity is lower (Fig. S3aS7a). The small peak at ca. 110 nm could be generated by heterogeneous nucleation of semi-volatile organic compounds mostly on primary carbonaceous aggregates (soot particles), which is a likely process in rapidly diluting and cooling air due to the turbulence caused by road vehicles. It could equally be a modelling artefact since in this diameter range, enlarged displacement intervals happened.

359

360 This factor is interpreted as atmospheric nucleation that is a combination of photochemically induced  
361 nucleation with traffic-related nucleation. The former process occurs on regional or urban spatial scales  
362 around noon. ~~In our results, this was also associated with strong southern winds (Fig. S9S19) consistently  
363 with our earlier conclusions (Németh and Salma, 2014). Higher WS values often represent cleaner air in  
364 the city centre, and the relationship between high WS and NPF occurrence is in line with our earlier  
365 observations in Budapest (Salma et al., 2021).~~ The traffic-related nucleation in cities can happen when  
366 the gas-phase vapours and gases in the exhaust of vehicles cool, and the resulted supersaturated vapours  
367 nucleate likely near, but outside the source (Charron and Harrison, 2003; Kittelson et al., 2022). The  
368 process yields particles which may be called primary because they form upon dilution of the exhaust  
369 plume, but have been also called delayed primary particles (Rönkkö et al., 2017) since they are generated  
370 outside the source (tailpipe). This explains why the traffic circulation patterns showed up in the time series  
371 of this factor.

372

373 The nucleation source in spring (when its relative occurrence frequency is the largest) was associated with  
374 S and SE direction and with high WS (Fig. S19). This conclusion is consistent with our earlier findings  
375 (Németh and Salma, 2014). Higher WS values often represent cleaner air in the city centre, and the  
376 relationship between the high WS and NPF occurrence is in line with our earlier observations in Budapest  
377 (Salma et al., 2021). In winter, its source directionality plot was featureless.

### 378 3.2.2 Traffic emissions

379 There were two factors showing unimodal source profile each in the Aitken mode, which indicates that  
380 these were primary particles (Figs. 3a and 4a). Both factors were strongly associated with NO, NO<sub>2</sub> and  
381 CO as well. ~~Both factors exhibited considerable contributions to NO, NO<sub>2</sub> and CO as well.~~ These gases  
382 are related to combustion processes. The time series of the concentration contributions of the two factors  
383 clearly followed the daily pattern of the vehicle circulation in Budapest, and were larger on weekdays  
384 than on weekends (Figs. 3c, 4c, S4-S8a, d and S5S9a, d). They both can be related to direct emissions  
385 from road vehicles with internal combustion engine. There were, however, several differences between  
386 the two factors, which discriminate them from each other.

387

388 One of the road traffic emission factors showed the largest contributions to the particles with a diameter  
389 of 25–35 nm (Fig. 3a). Its concentration contributions resulted in a mode, which was the smallest in  
390 summer (Fig. 3b). The diel variability of the factor also showed different magnitudes over seasons. The  
391 seasons were characterised by diverse seasonal mean  $T$  values from 3 to 23 °C (Table S2). The

392 contributions to the total particles were the largest in winter, large in autumn and spring, and the smallest  
 393 in summer (Fig. 3c). This points to the presence of chemical constituents with semi-volatile  
 394 physicochemical properties. The curves for summer contained a midday peak in addition to the rush-hour  
 395 peaks, which could be related to the altered traffic pattern (with a peak at noon) in Budapest on summer  
 396 holidays.

397

398

399

400

401

402

403

404

405

406

407

408

409

410

411

412

413

414

415

416

417

418

419

420

421

422

423

424

425

426

427

428

429

430

431

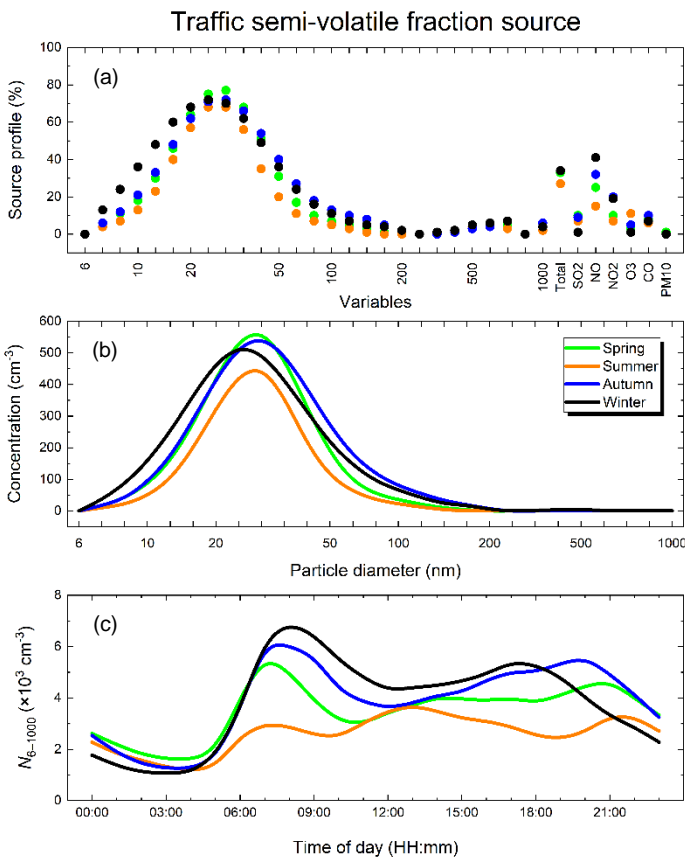


**Figure 3.** Relative factor profile (a), factor contribution to the particle number concentrations in the size channels (b), and the mean diel variation of the total particle number ( $N_{6-1000}$ ; c) assigned to the source of semi-volatile aerosol species emitted by road vehicle traffic (traffic-svf) in the uncorrected PMF modelling for spring, summer, autumn and winter. The exact diameters of the size channels are listed in Sect. 2.1.

Based on these reasons and consistently with earlier conclusions (Robinson et al., 2007; Morawska et al., 2008; Rönkkö et al., 2017; Harrison et al., 2018; Kittelson et al., 2022; Rowell et al., 2024), this factor is interpreted as emission source of semi-volatile aerosol fraction from road vehicle traffic (traffic-svf). Considering that diesel vehicles are responsible for much of the exhausted particle numbers from road traffic in Europe (Damayanti et al., 2023), the important concrete source is the emissions from diesel engines. The emissions from gasoline combustion in spark ignition engines likely contribute as well, which can be inferred from the differences in the diel patterns of the two traffic-related emission sources over the week (Figs. S4a-S8a vs. S5a-S9a). The naming and detailed interpretation of this factor vary in

432 the literature such as emissions from gasoline vehicles (Liu et al., 2014) or fresh traffic emissions (Rivas  
 433 et al., 2020) or Traffic 1 (Hopke et al., 2022).

434

435 The other road traffic emission factor yielded a source profile in a broader diameter interval, actually with  
 436 a plateau over 65–140 nm, than the traffic-svf source (Fig. 4a). The factor was also considerably  
 437 associated with SO<sub>2</sub> and PM<sub>10</sub> mass. ~~The factor also yielded higher contributions to SO<sub>2</sub> and PM<sub>10</sub> mass.~~  
 438 Its contributions to particle size channels exhibited a single mode with a diameter of 90 nm, which were  
 439 more stable over the seasons as far as the magnitude and shape are concerned (Fig. 4b). The shares of this  
 440 factor on the  $N_{6-1000}$  did not seem to be influenced by the  $T$  in various seasons (Fig. 4c).

441

442

443

444

445

446

447

448

449

450

451

452

453

454

455

456

457

458

459

460

461

462

463

464

465

466

467

468

469

470

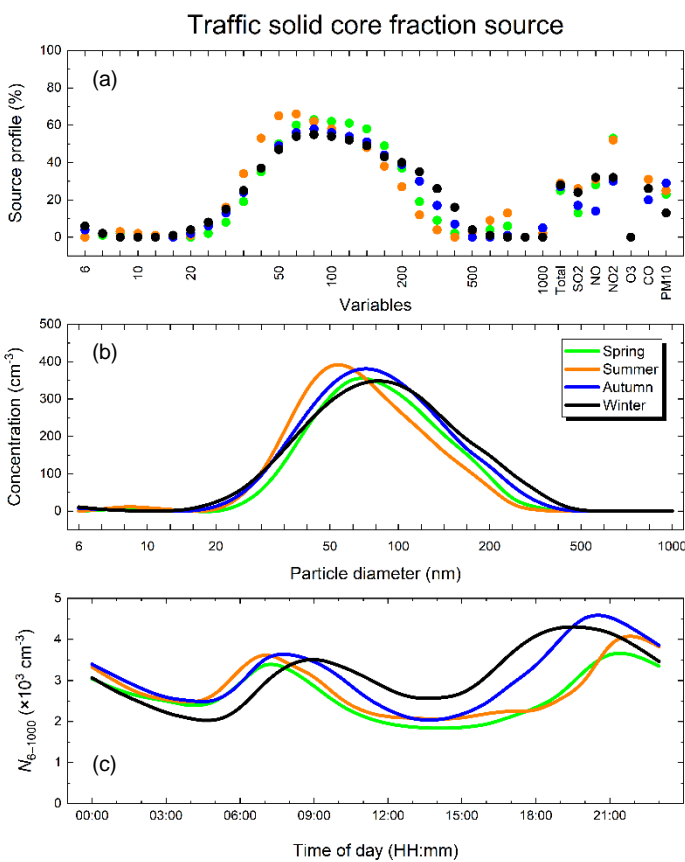
471

472

473

474

475



467 **Figure 4.** Relative factor profile (a), factor contribution to the particle number concentrations in the size channels (b), and the  
 468 mean diel variation of the total particle number ( $N_{6-1000}$ ; c) assigned to the source of solid aerosol species emitted by road  
 469 vehicle traffic (traffic-sf) in the uncorrected PMF modelling for spring, summer, autumn and winter. The exact diameters of  
 470 the size channels are listed in Sect. 2.1.

471

472 Based on these reasons and consistently with the earlier studies (Maricq et al., 2002; Rönkkö et al., 2017;  
 473 Kittelson et al., 2022; Damayanti et al., 2023; Rowell et al., 2024), this factor is interpreted as the source  
 474 of solid aerosol species emitted by road vehicle traffic (traffic-sf). These particles likely consist of a  
 475 carbonaceous aggregate (soot) or metal core coated with varying amounts of low-volatility organic and



476 inorganic compounds. Under some conditions, the metal compounds are even stick on the soot particles  
477 (Kittelson et al., 2022). The most important source contributing to this factor are the emissions from  
478 heavy- and light-duty vehicles (Zhang et al., 2020), which typically contain diesel-powered engine in  
479 Hungary. Chemically and physically aged traffic particles can be partly involved as well (Robinson et al.,  
480 2007). The naming and the detailed interpretation of this factor vary in the literature, e.g., emissions from  
481 diesel vehicles (Ogulei et al., 2007) or Traffic 2 (Hopke et al., 2022).

482  
483 Both traffic emission sources were related to local spatial scales in all seasons except for summer (Fig.  
484 S19). In the latter case, more distant regions and larger WS values prevailed. The source origin was related  
485 to smaller WS particularly in winter, and was shifted to more regional scales with WS in spring.

### 486 3.2.3 Diffuse urban source

487 Another factor showed a profile with broad peaks at ca. 100 nm and 500 nm (Fig. S6aS10a). It also  
488 contained several air pollutants including PM<sub>10</sub> mass (typically in 30 %, and up to 50 % in winter) and  
489 combustion-related pollutants such as CO, SO<sub>2</sub>, NO and NO<sub>2</sub>. The profile and contributions also included  
490 a low portion of smaller particles (around  $d = 20$  nm). The concentration contributions exhibited  
491 structured multiple peaks between 70 and 500 nm, which showed elevated levels in winter and autumn,  
492 and low values in summer and spring (Fig. S6bS10b). Its diel variations from spring to autumn displayed  
493 an early-morning peak and an evening peak (with higher level in autumn and lower levels in spring and  
494 summer). This pattern could be related to secondary particle formation from gas-phase precursors present  
495 in vehicle exhaust when it is fully diluted within the ambient air and oxidised by reactive atmospheric  
496 species. In such cases, the particles can grow by condensation. In winter, its diel variation was at the  
497 highest level and was eventually featureless (Fig. S6eS10c).

498  
499 Based on these considerations and earlier studies (Beddows et al., 2015; Beddows and Harrison, 2019;  
500 Chandrasekaran et al., 2011; Vratolis et al., 2019; Wang, K. et al., 2019), this factor is interpreted as  
501 source of diffuse (fugitive) urban aerosol. Important concrete sources contributing to it are aged  
502 combustion emissions from various boilers and heating equipment used for residential heating or food  
503 cooking. Burning residual oil and flaming combustion of solid fuels produce distributions with a modal  
504 diameter at approximately 100 nm, while efficient combustion of gases and low viscosity oil in stationary  
505 burners generate smaller particles (with a diameter at ca. 20 nm; Hopke et al., 2022 and references  
506 therein). In principle, resuspension of road and soil dust particles could also add (Conte et al., 2019) as a  
507 minor contributor in Budapest. This factor was called as urban background (Beddows and Harrison, 2019)  
508 or heating (Hopke et al., 2022).

509

510 The factor was linked to local spatial scales and low WS in all seasons (Fig. S9S19), which is in  
511 accordance with its interpretation.

### 512 3.2.4 Secondary inorganic aerosol

513 One of the further factors exhibited a source profile with a relatively narrow mode at the diameter of 800–  
514 1000 nm and a broad mode from 50 to 150 nm (Fig. S7aS11a). The mode with the larger diameter was  
515 present in all seasons with similar shapes to each other, but its concentration contributions were negligible  
516 (Fig. S7bS11b). The smaller-diameter mode in the source profile was the highest in spring, lower in  
517 summer and missing in autumn and winter (Fig. S7aS11a). Its concentration contributions in the size  
518 channels were modest. The shares over a broad size range from 30 to 170 nm were larger with a maximum  
519 of  $120 \text{ cm}^{-3}$  in spring, and with  $70 \text{ cm}^{-3}$  in summer (Fig. S7bS11b). The corresponding contributions in  
520 autumn and winter were negligible.

521

522 Based on these reasons and earlier results (Squizzato et al., 2019; Hopke et al., 2022 and references  
523 therein), this factor is ascribed to the sources of secondary inorganic aerosol (SIA), essentially containing  
524 sulfate and nitrate particles. An important concrete source could be their secondary formation from  
525 gaseous precursors in motor vehicles exhaust (Yoshizumi, 1986). The sulfate particles in the air are  
526 produced in a size mode around 100 nm preferably in summer and spring, when the photochemical  
527 activity is larger (Yoshizumi, 1986). Consequently, their formation in winter is lower. The ammonium  
528 nitrate particles behave contrary to this. They are mainly present in a size mode at ca. 250 nm and in  
529 winter, when the thermal dissociation of ammonium nitrate is low and (Kadowaki, 1977; Squizzato et al.,  
530 2019). The seasonal tendencies and size modes suggest that sulfate particles prevailed to nitrate particles  
531 in Budapest.

532

533 The multimodal directionality plots can indicate the presence of particles of both local and more distant  
534 origin. The latter particles were likely influenced by gas-to-particle conversion or other atmospheric or  
535 cloud processing (Ogulei et al., 2007; Kasumba et al., 2009; Squizzato et al., 2019). The SIA was mainly  
536 relevant in spring and summer (see Sect. 3.3), with prevailing SE and possibly NW directions,  
537 respectively and with high WS values (Fig. S19).

### 538 3.2.5 Secondary aerosol associated with high-ozone conditions

539 There was a factor associated with remarkably high  $\text{O}_3$  (> 80 %) and high  $\text{SO}_2$  (40 %–60 %) contents. It  
540 also showed a major mode in the size channels at ca. 200 nm in summer (Fig. S8aS12a). The

541 corresponding mode in spring was also present, but its contributions in autumn and winter became  
542 smaller.~~The corresponding mode in spring was also present, but it became negligible in autumn and~~  
543 ~~winter.~~ This could be caused by the large seasonal variability of O<sub>3</sub> in Budapest (Salma et al., 2020). As  
544 far as the factor contributions are concerned, they exhibited a mode at ca. 45 nm in winter and autumn,  
545 and a different mode at 150–200 nm in summer and spring (Fig. ~~S8b~~S12b). However, the absolute  
546 concentration contributions to the size channels remained extremely low (< 85 cm<sup>-3</sup>). These properties  
547 are in accordance with earlier studies, in which a variety of size patterns with multiple modes were  
548 obtained (Ogulei et al., 2007; Liu et al., 2014; Squizzato et al., 2019). The diel variation of the factor  
549 intensity during the daylight period was similar to the typical daily in situ development of O<sub>3</sub> in cities  
550 (Fig. ~~S8e~~S12c), and the contributions were higher on weekdays compared to weekends. The intensity of  
551 the O<sub>3</sub>-associated secondary aerosol source in winter and autumn remained low in the city centre and  
552 higher in its outskirts. The directionality plots indicated associations with higher WS (Fig. ~~S9~~S19).

553

554 This factor cannot be strictly interpreted in a conclusive manner. It is thought to be an appearance of the  
555 particles of various origin that were grown by condensation of vapours generated by photochemical  
556 oxidation driven by O<sub>3</sub> (Juozaitis et al., 1996; Hopke et al., 2022). This source may contain substantial  
557 fraction of organic compounds. Additional input data on chemical composition would be advantageous  
558 to clarify this factor. It was called O<sub>3</sub>-rich secondary aerosol in earlier studies (Ogulei et al., 2007; Liu et  
559 al., 2014; Squizzato et al., 2019).

### 560 3.3 Relevance of the dispersion correction

561 The seasonal median uncorrected modelled total particle number concentrations were 7.1, 6.8, 8.2 and  
562 7.8×10<sup>3</sup> cm<sup>-3</sup> from spring to winter. The corresponding corrected values were 9.2, 8.6, 10.3 and 9.9×10<sup>3</sup>  
563 cm<sup>-3</sup>. The correction did not considerably change the source profiles as far as both their structure and  
564 modal properties are concerned. The associations of air pollutants to the sources were altered somewhat  
565 more in a few isolated cases, but they are weak auxiliary variables. This is demonstrated for the 3 main  
566 sources (cf. Figs. 2a–4a with Figs. S13a–S15a). The shapes of the source contributions also remained  
567 virtually unchanged, but the magnitudes were modified and the curves for summer and spring were  
568 separated from the lines for autumn and winter (cf. Figs. 2b–4b with Figs. S13b–S15b). These changes  
569 are to be interpreted together with the alterations in the seasonal total particle number concentrations  
570 caused also by the dispersion correction. Their combined effect is captured by the mean relative  
571 concentration contributions of the sources, which is an expressive quantity.

572

573 The effect of the dispersion correction on the seasonal mean relative source contributions is shown in Fig.  
574 5. The correction increased the contribution of the nucleation from 20 % to 24 %, thus by a relative ratio  
575 of 23 % on an annual basis. The ratio was the largest (27 %) in winter and the smallest (18 %) in summer.  
576 The dispersion correction was relevant for the nucleation source, which photochemically driven  
577 component usually takes place in the midday period. At the same time, the correction did not alter the  
578 contributions of the traffic sources. Larger differences were observed for the low (<≈ 10 %) contributions,  
579 but these results raise the question of interpreting ratios obtained from small absolute values.

580  
581 The mean diel variations of the source types for uncorrected PMF and DC-PMF modelling are  
582 summarised in Figs. S16–S18 for separate seasons. For all sources, the corresponding curves essentially  
583 exhibited the same time patterns, while they were vertically shifted to higher or lower levels from each  
584 other. There were no obvious tendencies in the extent and directions of the shifts, except for the  
585 nucleation, which all corrected curves were above the uncorrected lines.

586  
587 It was demonstrated earlier (e.g., for Budapest lastly in Salma et al., 2020) that the local meteorological  
588 properties can influence the ambient atmospheric concentrations and size distributions in cities in a  
589 comparable extent than the changes in the source intensities (Li et al., 2023). The dispersion correction  
590 was dedicatedly introduced to remove a large part of the extra covariance between the variables, which is  
591 frequently or enduringly caused by the common effect of the meteorology on all concentrations. This  
592 basic motivation already implies that the corrected concentrations and concentration contributions are  
593 expected to be closer to reality and of higher reliability than their uncorrected counterparts. At the same  
594 time, the correction did not considerably alter the source profiles, temporal behaviours and patterns.  
595 Furthermore, some previous papers have also demonstrated the value of the dispersion correction in  
596 estimating the source contributions (e.g., Dai et al., 2020, 2021; Hopke et al., 2024).

597  
598 ~~The conditional bivariate probability plots of the outcomes~~ obtained from the both uncorrected PMF and  
599 DC-PMF modelling-models indicated qualitatively comparable properties and behaviours to each  
600 otherthem. The differences in the directionality plots were obtained by subtracting the uncorrected PMF  
601 results from the DC-PMF results (Fig. S9S19). ~~The road vehicle traffic emission sources were related to~~  
602 ~~local spatial scales in all seasons except for summer. In the latter case, more distant regions and larger~~  
603 ~~WS values prevailed. The nucleation source in spring (when its occurrence frequency is the largest) was~~  
604 ~~associated with SE direction and high WS. This directionality is coherent with our earlier finding (Németh~~  
605 ~~and Salma, 2014). In winter, its source directionality plots were featureless. The diffuse urban aerosol~~

606 ~~originated from local spatial scales and low WS in all seasons, which is in accordance with its source~~  
607 ~~interpretation. The SIA was relevant only in spring and summer, with prevailing SE and NW directions,~~  
608 ~~respectively and with high WS values. The intensity of the O<sub>3</sub>-associated secondary aerosol source in~~  
609 ~~winter and autumn remained low in the city centre and higher in its outskirt.~~

610  
611 ~~Despite the similar seasonal mean contributions from both the uncorrected and corrected PMF (Fig. 5),~~  
612 ~~there are substantial variations in the plots.~~ The corrected PMF could change the source origins in many  
613 cases. In this respect, the DC-PMF can also provide important added values on the spatial distributions.  
614 More interpretations will be feasible-available after gaining further experience and expertise in the future  
615 studies.

### 616 **3.3.4 Importance of the sources**

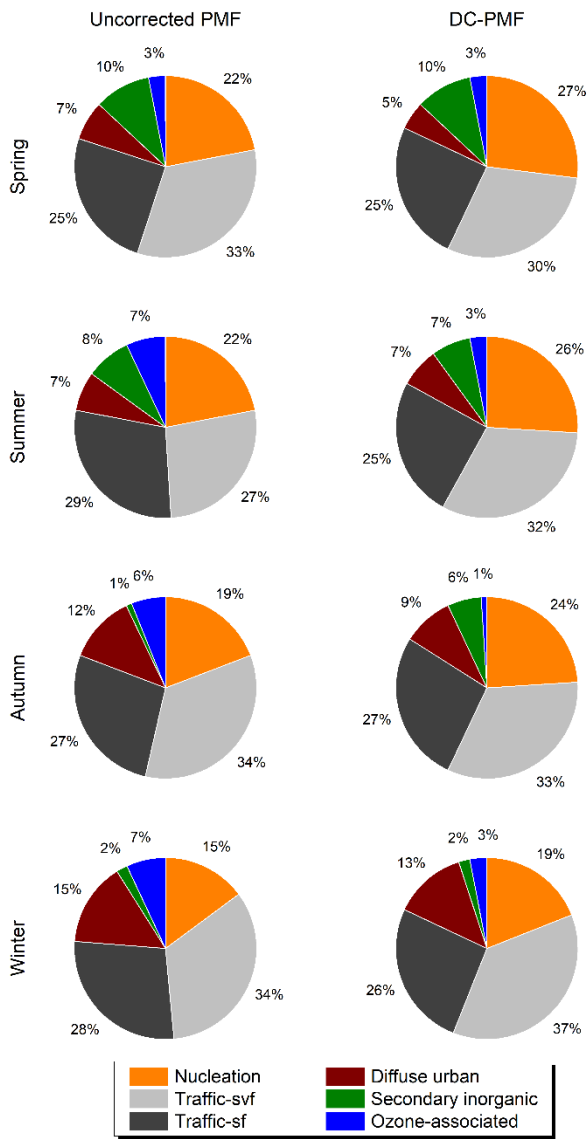
617 The mean relative contributions of the sources to the total modelled concentrations derived by both the  
618 uncorrected PMF and DC-PMF approaches are displayed in Fig. 5 in separate seasons. The relative  
619 contributions of unaccounted sources with respect to the measured  $N_{6-1000}$  were estimated to be  $\approx 2\%$ .

620 It is the DC-PMF results that are interpreted here because they are expected to be more reliable than the  
621 uncorrected results as shown in Sect. 3.3.

622  
623 The overall mean relative contribution of the road vehicle traffic emissions was 59 %; 32-33 % for traffic-  
624 svf and 27-26 % for traffic-sf. The latter source did not show ~~clear~~ tendency in the seasonal variability-  
625 T, while the former source traffic-svf could be was somewhat enhanced in winter due possibly to lower  
626 ambient T in this season (Table S2). The values seem to be in line with those in other large cities (Beddows  
627 et al., 2015; Brines et al., 2015; Dall'Osto et al., 2012; Liu et al., 2014; Posner and Pandis, 2015; Squizzato  
628 et al., 2019; Rivas et al., 2020, Hopke et al., 2022 and references therein). Despite the fact that the  
629 emissions from vehicles depend on multiple conditions, for instance on the car fleet, general technical  
630 conditions of vehicles, properties of fuels and lubricants used, driving conditions, ambient T, RH and  
631 even on the distance to the nearest road (Rönkkö et al., 2017; Kittelson et al., 2022).

632

633  
634  
635  
636  
637  
638  
639  
640  
641  
642  
643  
644  
645  
646  
647  
648  
649  
650  
651  
652  
653  
654  
655  
656  
657  
658  
659  
660  
661  
662  
663  
664  
665



666 **Figure 5.** Mean relative contributions of the nucleation, road vehicle traffic semi-volatile fraction (traffic-svf), road vehicle  
667 traffic solid core fraction (traffic-sf), diffuse urban, secondary inorganic aerosol and ozone-associated secondary aerosol  
668 sources to the modelled total particle number concentrations as obtained by the uncorrected PMF modelling (left column) and  
669 the dispersion-corrected (DC-)PMF modelling (right column) in spring, summer, autumn and winter.

670

671 The nucleation source was responsible for 20–24 % of the particle numbers annually. It was the largest  
672 (27 %) in spring and the smallest (19 %) in winter ~~smaller in winter than in the other seasons, particularly~~  
673 ~~compared to the spring and summer.~~ This seasonal tendency is partially linked to the monthly distribution  
674 of the NPF event occurrence frequency (which has a maximum in spring and a minimum in winter in the  
675 Budapest area; Salma et al., 2021). The overall share of the nucleation was comparable to our earlier  
676 conclusion of 12 %–27 % (to UF particles) as a lower assessment ~~provided~~ derived by the nucleation  
677 strength factor, and ~~to~~ by other ~~implicit~~ indirect indications (Salma et al., 2017; Thén and Salma, 2022).  
678 The present contribution can be, however, considered again as a lower estimate since an extensive portion  
679 produced by some other source types can be also related to the nucleation. This is the case particularly



680 for the SIA in summer and spring, and possibly also for the urban diffuse source in winter and autumn.  
681 The former source could partly contribute to the nucleation through the vapours generated from gaseous  
682 precursors (such as SO<sub>2</sub> and volatile organics) and H<sub>2</sub>SO<sub>4</sub>(~~including SO<sub>2</sub>, H<sub>2</sub>SO<sub>4</sub> and volatile organics~~) in  
683 the exhausts of road vehicles, ships or airplanes, and in the fumes of coal-fired power plants. The urban  
684 diffuse source could be linked to nucleated particles via particle growth followed by physical and  
685 chemical ageing processes, and possibly coagulation. In addition, an unusual type of NPF events  
686 characterised by atypical time evolution and induced by some urban, industrial or leisure activities on  
687 sublocal or local spatial scales with extremely high formation rates are observed in Budapest not rarely  
688 (Salma and Németh, 2019), which can also add.

689

690 The contributions from the urban diffuse and SIA source types were the largest in autumn and winter, and  
691 in spring and summer, respectively (both with seasonal maxima of ca. 10 %).~~The contributions from the~~  
692 ~~SIA and urban diffuse source types were approximately 10 % in spring and summer, and 12–15 % in~~  
693 ~~autumn and winter, respectively. The O<sub>3</sub>-associated secondary aerosol made up the smallest (ca. 3 %)~~  
694 ~~mean contribution on an annual time scale. The shares of the SIA in winter and autumn were 2–3 %.~~The  
695 O<sub>3</sub>-associated secondary aerosol made up the smallest (≈ 36 %) mean share on an annual time scale.  
696 These tendencies are in line with our general understanding of the ~~time~~-behaviour on the related source  
697 processes and particles.

#### 698 **4 Conclusions**

699 Six main source types of particle numbers were identified in Budapest. The road vehicle emissions is the  
700 largest-leading contributor; they were responsible for approximately 60 % of particles. This source was  
701 resolved into a semi-volatile fraction and a solid core fraction. It seems likely that these two types do not  
702 express the emissions from gasoline- and diesel-driven motor vehicles, respectively, but they represent  
703 two distinct groups of chemical mixtures from both internal combustion engines. Nevertheless, both  
704 traffic emission sources, particularly that which containing contains solid core fraction, are dominated by  
705 diesel motor vehicles. More importantly, the latter source is characterised by a relatively large modal  
706 diameter of 90 nm, and is expected to contain high portions of insoluble particles. These properties can  
707 yield considerably larger lung deposited surface areas than for the traffic-svf or the other sources (except  
708 for the urban diffuse source), which results in extraordinary particle burden in the human lung caused by  
709 this single source. Furthermore, the surface-active properties of the soot core likely represent additional  
710 risk for the health outcomes.

711

712 The nucleation source was responsible for ca. ~~20–24~~ % of particles as a lower estimate. It displayed a  
713 compound character consisting of photochemically induced nucleation and traffic-related nucleation.  
714 There is a method available for splitting it into the two specific subfactors using NO<sub>x</sub> as a proximity  
715 marker for road vehicle traffic (Rivas et al., 2020). However, in our datasets the coefficients of correlation  
716 between the concentration contribution of the nucleation source and NO<sub>x</sub> concentration were typically <  
717 0.2, and adopting this method yielded unusually small photochemically induced nucleation contributions.  
718 These findings are in contrast with our earlier results and other indirect estimations, and with other  
719 suggestions as well. Furthermore, the shares of the two subfactors are expected to depend also on several  
720 other traffic and environmental conditions such as the characteristics of the vehicle fleet, ambient T, RH,  
721 GRad or background particle concentration. Therefore, we avoided adopting this estimation for the time  
722 of being, and emphasize here the need for developing generally valid splitting methods, and testing them  
723 on a variety of datasets.

724

725 The relatively large modal diameter of the abundant traffic solid core fraction source also stimulates the  
726 question whether the upper diameter limit of the UF particles is set at a correct value. Some important  
727 health-related metrics such as the surface area of particles or the lung deposited surface area size  
728 distributions can largely extend above the traditional 100-nm threshold. The outlying upper part of these  
729 exposure indicators can confuse or obscure the studies of particle exposures on the human health. The  
730 particle number size distributions attributed to separate sources together with their conjugate size  
731 distributions over the whole particle diameter range are to be further utilised in an advanced lung  
732 deposition model for characterising and quantifying source specific depositions in the human respirators  
733 system.

734 *Data availability.* The observational data are available from the corresponding author (IS).

735 *Supplement.* The supplement related to this article is available online at: *to be completed.*

736 *Author contributions.* MV performed the data treatment and modelling, prepared the figures, participated in the interpretation  
737 and writing the manuscript. PKH participated in the conceptualization, the interpretation of the results and editing. IS provided  
738 the dataset, conducted the conceptualization, participated in the interpretation and writing the manuscript. All coauthors  
739 contributed to the discussion of the results and provided comments on the manuscript.

740 *Competing interests.* One coauthor (IS) is member of the editorial board of Atmospheric Chemistry and Physics. The authors  
741 declare that they have no conflict of interest.

742 *Financial support.* This research has been supported by the Hungarian Research, Development and Innovation Office (grant  
743 K132254), and the New National Excellence Program of the Ministry for Culture and Innovation from the source of the  
744 National Research, Development and Innovation Fund (ÚNKP-22-3).

745 **References**

- 746 Andronabusche, C.: Precipitation removal of ultrafine aerosol particles from the atmospheric boundary layer, *J. Geophys.*  
747 *Res.*, 109, D16S07, <https://doi.org/10.1029/2003jd004050>, 2004.
- 748 Ashrafi, Kh., Shafie-Pour, M., and Kamalan, H.: Estimating temporal and seasonal variation of ventilation coefficients, *Int.*  
749 *J. Environ. Res.*, 3, 637–644, 2009.
- 750 Beddows, D. C. S., Harrison, R. M., Green, D. C., and Fuller, G. W.: Receptor modelling of both particle composition and  
751 size distribution from a background site in London, UK, *Atmos. Chem. Phys.*, 15, 10107–10125,  
752 <https://doi.org/10.5194/acp-15-10107-2015>, 2015.
- 753 Beddows, D. C. S. and Harrison, R. M.: Receptor modelling of both particle composition and size distribution from a  
754 background site in London, UK – a two-step approach, *Atmos. Chem. Phys.*, 19, 4863–4876, <https://doi.org/10.5194/acp-19-4863-2019>, 2019.
- 756 [Belis, C. A., Pernigotti, D., Pirovano, G., Favez, O., Jaffrezo, J. L., Kuenen, J., Denier van Der Gon, H., Reizer, M., Riffault, V., Alleman, L. Y., Almeida, M., Amato, F., Angyal, A., Argyropoulos, G., Bande, S., Beslic, I., Besombes, J.-L., Bove, M. C., Brotto, P., Calori, G., Cesari, D., Colombi, C., Contini, D., De Gennaro, G., Di Gilio, A., Diapouli, E., El Haddad, I., Elbern, H., Eleftheriadis, K., Ferreira, J., Vivanco, M. G., Gilardoni, S., Golly, B., Hellebust, S., Hopke, P. K., Izadmanesh, Y., Jorquera, H., Krajsek, K., Kranenburg, R., Lazzeri, P., Lenartz, F., Lucarelli, F., Maciejewska, K., Manders, A., Manousakas, M., Masiol, M., Mircea, M., Mooibroek, D., Nava, S., Oliveira, D., Paglione, M., Pandolfi, M., Perrone, M., Petralia, E., Pietrodangelo, A., Pillon, S., Pokorna, P., Prati, P., Salameh, D., Samara, C., Samek, L., Saraga, D., Sauvage, S., Schaap, M., Scotto, F., Sega, K., Siour, G., Tauler, R., Valli, G., Vecchi, R., Venturini, E., Vestenius, M., Waked, A., and Yubero, E.: Evaluation of receptor and chemical transport models for PM<sub>10</sub> source apportionment, \*Atmos. Environ.\* X, 5, 100053, doi:10.1016/j.aeoa.2019.100053, 2020.](#)
- 766 Braakhuis, H. M., Park, M. V., Gosens, I., De Jong, W. H., and Cassee, F. R.: Physicochemical characteristics of  
767 nanomaterials that affect pulmonary inflammation, *Part. Fibre Toxicol.*, 11, 18, <https://doi.org/10.1186/1743-8977-11-18>,  
768 2014.
- 769 Brines, M., Dall'Osto, M., Beddows, D. C. S., Harrison, R. M., Gómez-Moreno, F., Núñez, L., Artíñano, B., Costabile, F.,  
770 Gobbi, G. P., Salimi, F., Morawska, L., Sioutas, C., and Querol, X.: Traffic and nucleation events as main sources of  
771 ultrafine particles in high insolation developed world cities, *Atmos. Chem. Phys.*, 15, 5929–5945.  
772 <https://doi.org/10.5194/acp-15-5929-2015>, 2015.
- 773 Carslaw, D. C. and Ropkins, K.: openair – An R package for air quality data analysis, *Environ. Modell. Softw.*, 27–28, 52–  
774 61, <https://doi.org/10.1016/j.envsoft.2011.09.008>, 2012.
- 775 Chalupa, D. C., Morrow, P. E., Oberdörster, G., Utell, M. J., and Frampton, M. W.: Ultrafine particle deposition in subjects  
776 with asthma, *Environ. Health Perspect.*, 112, 879–882, <https://doi.org/10.1289/ehp.6851> 879–882, 2004.
- 777 Chandrasekaran, S. R., Laing, J. R., Holsen, T. M., Raja, S., and Hopke, P. K.: Emission characterization and efficiency  
778 measurements of high-efficiency wood boilers, *Energy Fuels* 25, 5015–5021, <https://doi.org/10.1021/ef2012563>, 2011.
- 779 Charron, A. and Harrison, R. M.: Primary particle formation from vehicle emissions during exhaust dilution in the roadside  
780 atmosphere, *Atmos. Environ.*, 37, 4109–4119, [https://doi.org/10.1016/S1352-2310\(03\)00510-7](https://doi.org/10.1016/S1352-2310(03)00510-7), 2003.
- 781 [Conte, M. and Contini, D.: Size-resolved particle emission factors of vehicular traffic derived from urban eddy covariance measurements, \*Environ. Pollut.\*, 251, 830–838, <https://doi.org/10.1016/j.envpol.2019.05.029>, 2019.](#)
- 783 Conte, M., Dinoi, A., Grasso, F. M., Merico, E., Guascito, M. R., and Contini, D.: Concentration and size distribution of  
784 atmospheric particles in southern Italy during COVID-19 lockdown period, *Atmos. Environ.*, 295, 119559,  
785 <https://doi.org/10.1016/j.atmosenv.2022.119559>, 2023.
- 786 Corsini, E., Marinovich, M., and Vecchi, R.: Ultrafine particles from residential biomass combustion: A review on  
787 experimental data and toxicological response, *Int. J. Mol. Sci.*, 20, 4992, <https://doi.org/10.3390/ijms20204992>, 2019.
- 788 Crova, F., Forello, A. C., Bernardoni, V., Calzolari, G., Canepari, S., Argentini, S., Costabile, F., Frezzini, M. A., Giardi, F.,  
789 Lucarelli, F., Massabò, D., Massimi, L., Nava, S., Paglione, M., Pazzi, G., Prati, P., Rinaldi, M., Russo, M., Valentini, S.,  
790 Valli, G., Vernocchi, V., and Vecchi, R.: Assessing the role of atmospheric dispersion vs. emission strength in the  
791 southern Po Valley (Italy) using dispersion-normalised multi-time receptor modelling, *Atmos. Environ.*, 316, 120168,  
792 <https://doi.org/10.1016/j.atmosenv.2023.120168>, 2024.
- 793 Dai, Q., Hopke, P. K., Bi, X., and Feng, Y.: Improving apportionment of PM<sub>2.5</sub> using multisite PMF by constraining G-  
794 values with apriori information, *Sci. Total Environ.*, 736, 139657, <https://doi.org/10.1016/j.scitotenv.2020.139657>, 2020.

795 Dai, Q., Ding, J., Song, C., Liu, B., Bi, X., Wu, J., Zhang, Y., Feng, Y., and Hopke, P. K.: Changes in source contributions to  
796 particle number concentrations after the COVID-19 outbreak: Insights from a dispersion normalized PMF, *Sci. Total*  
797 *Environ.*, 759, 143548, <https://doi.org/10.1016/j.scitotenv.2020.143548>, 2021.

798 Damayanti, S., Harrison, R. M., Pope, F., and Beddows, D. C. S.: Limited impact of diesel particle filters on road traffic  
799 emissions of ultrafine particles, *Environ. Int.*, 174, 107888, <https://doi.org/10.1016/j.envint.2023.107888>, 2023.

800 de Jesus, A. L., Thompson, H., Knibbs, L. D., Kowalski, M., Cyrus, J., Niemi, J. V., Kousa, A., Timonen, H., Luoma, K.,  
801 Petäjä, T., Beddows, D., Harrison, R. M., Hopke, P., and Morawska, L.: Long-term trends in PM<sub>2.5</sub> mass and particle  
802 number concentrations in urban air: the impacts of mitigation measures and extreme events due to changing climates,  
803 *Environ. Pollut.*, 263, 114500, <https://doi.org/10.1016/j.envpol.2020.114500>, 2020.

804 EU EEA: Air pollution, <https://www.eea.europa.eu/en/topics/in-depth/air-pollution> (last access: 20 December 2023), 2023.

805 Harni, S. D., Aurtela, M., Saarikoski, S., Niemi, J., Portin, H., Manninen, H., Leinonen, V., Aalto, P., Hopke, P., Petäjä, T.,  
806 Rönkkö, T., and Timonen, H.: Source apportionment of particle number size distribution at the street canyon and urban  
807 background sites, *EGUsphere* [preprint], <https://doi.org/10.5194/egusphere-2023-2428>, 2023.

808 Harrison, R. M., Beddows, D. C. S., and Dall'Osto, M.: PMF analysis of wide-range particle size spectra collected on a  
809 major highway, *Environ. Sci. Technol.*, 45, 5522–5528, <https://doi.org/10.1021/es2006622>, 2011.

810 Harrison, R. M., MacKenzie, R. A., Xu, H., Alam, M. S., Nikolova, I., Zhong, J., Singh, A., Zeraati-Rezaei, S., Stark, C.,  
811 Beddows, D. C. S., Liang, Z., Xu, R., and Cai, X.: Diesel exhaust nanoparticles and their behaviour in the atmosphere,  
812 *Proc. R. Soc. A* 474, <https://doi.org/10.1098/rspa.2018.0492>, 2018.

813 Harrison, R. M., Beddows, D. C. S., Alam, M. S., Singh, A., Brean, J., Xu, R., Kotthaus, S., and Grimmond, S.:  
814 Interpretation of particle number size distributions measured across an urban area during the FASTER campaign, *Atmos.*  
815 *Chem. Phys.*, 19, 39–55, <https://doi.org/10.5194/acp-19-39-2019>, 2019.

816 HEI Review Panel on Ultrafine Particles: Understanding the health effects of ambient ultrafine particles, *HEI Perspectives* 3,  
817 Health Effects Institute, Boston, 2013.

818 Hersbach, H., Bell, B., Berrisford, P., Biavati, G., Horányi, A., Muñoz Sabater, J., Nicolas, J., Peubey, C., Radu, R., Rozum,  
819 I., Schepers, D., Simmons, A., Soci, C., Dee, D., and Thépaut, J.-N.: ERA5 hourly data on single levels from 1940 to  
820 present. Copernicus Climate Change Service (C3S) Climate Data Store (CDS), <https://doi.org/10.24381/cds.adbb2d47>  
821 (last access: 10 September 2023), 2023.

822 Holzworth, G. C.: Mixing depths, wind speeds and air pollution potential for selected locations in the United States, *J. Appl.*  
823 *Meteor.*, 6, 1039–1044, [https://doi.org/10.1175/1520-0450\(1967\)006<1039:mdwsaa>2.0.co;2](https://doi.org/10.1175/1520-0450(1967)006<1039:mdwsaa>2.0.co;2), 1967.

824 Hopke, P. K.: An introduction to receptor modeling, *Chemometr. Intell. Lab.*, 10, 21–43, [https://doi.org/10.1016/0169-7439\(91\)80032-1](https://doi.org/10.1016/0169-7439(91)80032-1), 1991.

825 Hopke, P. K.: A guide to positive matrix factorization. <https://people.clarkson.edu/~phopke/PMF-Guidance.htm> (last access:  
826 10 September 2023), 2000.

827 Hopke, P. K.: Review of receptor modeling methods for source apportionment, *J. Air Waste Manage.*, 66, 237–259,  
828 <https://doi.org/10.1080/10962247.2016.1140693>, 2016.

829 Hopke, P. K., Dai, Q., Li, L., and Feng, Y.: Global review of recent source apportionments for airborne particulate matter,  
830 *Sci. Total Environ.*, 740, 140091, <https://doi.org/10.1016/j.scitotenv.2020.140091>, 2020.

831 Hopke, P. K., Feng, Y., and Dai, Q.: Source apportionment of particle number concentrations: A global review, *Sci. Total*  
832 *Environ.*, 819, 153104, <https://doi.org/10.1016/j.scitotenv.2022.153104>, 2022.

833 Hopke, P. K., Chen, Y., Rich, D. Q., Mooibroek, D., and Sofowote, U. M.: The application of positive matrix factorization  
834 with diagnostics to BIG DATA, *Chemometr. Intell. Lab.*, 240, 104885, <https://doi.org/10.1016/j.chemolab.2023.104885>,  
835 2023.

836 [Hopke, P. K., Chen, Y., Chalupa, D. C., and Rich, D. Q.: Long term trends in source apportioned particle number](https://doi.org/10.1016/j.envpol.2024.123708)  
837 [concentrations in Rochester NY, \*Environ. Pollut.\*, 347, 123708, https://doi.org/10.1016/j.envpol.2024.123708, 2024.](https://doi.org/10.1016/j.envpol.2024.123708)

838 Ibald-Mulli, A., Wichmann, H.-E., Kreyling, W., and Peters, A.: Epidemiological evidence on health effects of ultrafine  
839 particles, *J. Aerosol Med.*, 15, 189–201, <https://doi.org/10.1089/089426802320282310>, 2002.

840 Juozaitis, A., Trakumas, S., Girgždien, R., Girgždys, A., Šopauskien, D., and Ulevičius, V.: Investigations of gas-to-particle  
841 conversion in the atmosphere, *Atmos. Res.*, 41, 183–201, [https://doi.org/10.1016/0169-8095\(96\)00008-7](https://doi.org/10.1016/0169-8095(96)00008-7), 1996.

842 Kadowaki, S.: Size distribution and chemical composition of atmospheric particulate nitrate in the Nagoya area, *Atmos.*  
843 *Environ.*, 11, 671–675, [https://doi.org/10.1016/0004-6981\(77\)90174-3](https://doi.org/10.1016/0004-6981(77)90174-3), 1977.

844

845 Kittelson, D., Khalek, I., McDonald, J., Stevens, J., and Giannelli, R.: Particle emissions from mobile sources: Discussion of  
846 ultrafine particle emissions and definition, *J. Aeros. Sci.*, 159, 105881, <https://doi.org/10.1016/j.jaerosci.2021.105881>,  
847 2022.

848 Kerminen, V. M., Chen, X., Vakkari, V., Petäjä, T., Kulmala, M., and Bianchi, F.: Atmospheric new particle formation and  
849 growth: Review of field observations, *Environ. Res. Lett.*, 13, 103003, <https://doi.org/10.1088/1748-9326/aadf3c>, 2018.

850 Ketznel, M. and Berkowicz, R.: Modelling the fate of ultrafine particles from exhaust pipe to rural background: an analysis of  
851 time scales for dilution, coagulation and deposition, *Atmos. Environ.*, 38, 2639–2652,  
852 <https://doi.org/10.1016/j.atmosenv.2004.02.020>, 2004.

853 Kreyling, W. G., Semmler-Behnke, M., and Möller, W.: Ultrafine particle-lung interactions: does size matter? *J. Aerosol*  
854 *Med.*, 19, 74–83, <https://doi.org/10.1089/jam.2006.19.74>, 2006.

855 Kumar, P., Ketznel, M., Vardoulakis, S., Pirjola, L., and Britter, R.: Dynamics and dispersion modelling of nanoparticles from  
856 road traffic in the urban atmospheric environment – A review, *J. Aerosol Sci.*, 42, 580–603,  
857 <https://doi.org/10.1016/j.jaerosci.2011.06.001>, 2011.

858 Kulmala, M.: How particles nucleate and grow, *Science*, 302, 1000, <https://doi.org/10.1126/science.1090848>, 2003.

859 Kulmala, M., Petäjä, T., Ehn, M., Thornton, J., Sipilä, M., Worsnop, D. R., and Kerminen, V. M.: Chemistry of atmospheric  
860 nucleation: On the recent advances on precursor characterization and atmospheric cluster composition in connection with  
861 atmospheric new particle formation, *Annu. Rev. Phys. Chem.*, 65, 21–37, <https://doi.org/10.1146/annurev-physchem-040412-110014>, 2014.

863 Kulmala, M., Lintunen, A., Lappalainen, H., Virtanen, A., Yan, C., Ezhova, E., Nieminen, T., Riipinen, I., Makkonen, R.,  
864 Tamminen, J., Sundström, A.-M., Arola, A., Hansel, A., Lehtinen, K., Vesala, T., Petäjä, T., Bäck, J., Kokkonen, T., and  
865 Kerminen, V.-M.: Opinion: The strength of long-term comprehensive observations to meet multiple grand challenges in  
866 different environments and in the atmosphere, *Atmos. Chem. Phys.*, 23, 14949–14971, <https://doi.org/10.5194/acp-23-14949-2023>, 2023.

868 Leahey, D. M.: An advective model for predicting air pollution within an urban heat island with applications to New York  
869 City, *J. Air Waste Manag. Assoc.*, 22, 548–550, <https://doi.org/10.1080/00022470.1972.10469678>, 1972.

870 Li, Q.-Q., Guo, Y.-T., Yang, J.-Y., and Liang, C.-S.: Review on main sources and impacts of urban ultrafine particles:  
871 Traffic emissions, nucleation, and climate modulation, *Atmos. Environ.: X*, 19, 100221,  
872 <https://doi.org/10.1016/j.aeaoa.2023.100221>, 2023.

873 Li, W. and Hopke, P. K.: Initial size distributions and hygroscopicity of indoor combustion aerosol particles, *Aerosol Sci.*  
874 *Technol.*, 19, 305–316, <https://doi.org/10.1080/02786829308959638>, 1993.

875 Liu, Z. R., Hu, B., Liu, Q., Sun, Y., and Wang, Y. S.: Source apportionment of urban fine particle number concentration  
876 during summertime in Beijing, *Atmos. Environ.*, 96, 359–369, <https://doi.org/10.1016/j.atmosenv.2014.06.055>, 2014.

877 Maricq, M. M., Chase, R. E., Xu, N., and Laing, P. M.: The effects of the catalytic converter and fuel sulfur level on motor  
878 vehicle particulate matter emissions: Light duty diesel vehicles, *Environ. Sci. Technol.*, 36, 283–289,  
879 <https://doi.org/10.1021/es010962l>, 2002.

880 Meng, X., Ma, Y., Chen, R., Zhou, Z., Chen, B., and Kan, H.: Size-fractionated particle number concentrations and daily  
881 mortality in a Chinese city, *Environ. Health Perspect.*, 121, 1174–1178, <https://doi.org/10.1289/ehp.1206398>, 2013.

882 Mikkonen, S., Németh, Z., Varga, V., Weidinger, T., Leinonen, V., Yli-Juuti, T., and Salma, I.: Decennial time trends and  
883 diurnal patterns of particle number concentrations in a central European city between 2008 and 2018, *Atmos. Chem.*  
884 *Phys.*, 20, 12247–12263, <https://doi.org/10.5194/acp-20-12247-2020>, 2020.

885 Morawska, L., Ristovski, Z., Jayaratne, E. R., Keogh, D. U., and Ling, X.: Ambient nano and ultrafine particles from motor  
886 vehicle emissions: Characteristics, ambient processing and implications on human exposure, *Atmos. Environ.*, 42, 8113–  
887 8138, <https://doi.org/10.1016/j.atmosenv.2008.07.050>, 2008.

888 Németh, Z. and Salma, I.: Spatial extension of nucleating air masses in the Carpathian Basin, *Atmos. Chem. Phys.*, 14,  
889 8841–8848, <https://doi.org/10.5194/acp-14-8841-2014>, 2014.

890 Oberdörster, G., Oberdörster, E., and Oberdörster, J.: Nanotoxicology: An emerging discipline evolving from studies of  
891 ultrafine particles, *Environ. Health Perspect.*, 113, 823–839, <https://doi.org/10.1289/ehp.7339>, 2005.

892 Ogulei, D., Hopke, P. K., Chalupa, D., and Utell, M.: Modeling source contributions to submicron particle number  
893 concentrations measured in Rochester, NY, *Aerosol Sci. Technol.*, 41, 179–201,  
894 <https://doi.org/10.1080/02786820601116012>, 2007.

895 Paatero, P.: The Multilinear Engine: A table-driven, least squares program for solving multilinear problems, including the n-  
896 way parallel factor analysis model, *J. Comput. Graph. Stat.*, 8, 854, <https://doi.org/10.2307/1390831>, 1999.

897 Paatero, P. and Tapper, U.: Analysis of different modes of factor analysis as least squares fit problems, *Chemometr. Intell.*  
898 *Lab.*, 18, 183–194, [https://doi.org/10.1016/0169-7439\(93\)80055-m](https://doi.org/10.1016/0169-7439(93)80055-m), 1993.

899 Paatero, P. and Tapper, U.: Positive matrix factorization: A non-negative factor model with optimal utilization of error  
900 estimates of data values, *Environmetrics*, 5, 111–126, <https://doi.org/10.1002/env.3170050203>, 1994.

901 Pandolfi, M., Gonzalez-Castanedo, Y., Alastuey, A., de la Rosa, J. D., Mantilla, E., de la Campa, A. S., Querol, X., Pey, J.,  
902 Amato, F., and Moreno, T.: Source apportionment of PM<sub>10</sub> and PM<sub>2.5</sub> at multiple sites in the strait of Gibraltar by PMF:  
903 impact of shipping emissions, *Environ. Sci. Pollut. Res.*, 18, 260–269, <https://doi.org/10.1007/s11356-010-0373-4>, 2010.

904 Riediker, M., Zink, D., Kreyling, W., Oberdörster, G., Elder, A., Graham, U., Lynch, I., Duschl, A., Ichihara, G., Ichihara,  
905 S., Kobayashi, T., Hisanaga, N., Umezawa, M., Cheng, T.-J., Handy, R., Gulumian, M., Tinkle, S., and Cassee, F.:  
906 Particle toxicology and health - where are we?, *Part. Fibre Toxicol.*, 16, <https://doi.org/10.1186/s12989-019-0302-8>,  
907 2019.

908 Rivas, I., Beddows, D. C. S., Amato, F., Green, D. C., Järvi, L., Hueglin, C., Reche, C., Timonen, H., Fuller, G. W., Niemi,  
909 J. V., Pérez, N., Aurela, M., Hopke, P. K., Alastuey, A., Kulmala, M., Harrison, R. M., Querol, X., and Kelly, F. J.:  
910 Source apportionment of particle number size distribution in urban background and traffic stations in four European  
911 cities, *Environ. Int.*, 135, 105345, <https://doi.org/10.1016/j.envint.2019.105345>, 2020.

912 Robinson, A. L., Donahue, N. M., Shrivastava, M. K., Weitkamp, E. A., Sage, A. M., Grieshop, A. P., Lane, T. E., Pierce, J.  
913 R., and Pandis, S. N.: Rethinking organic aerosols: semivolatile emissions and photochemical aging, *Science*, 80, 315,  
914 1259–1262, <https://doi.org/10.1126/science.1133061>, 2007.

915 Rowell, A., Brean, J., Beddows, D. C. S., Shi, Z., Petäjä, T., Vörösmarty, M., Salma, I., Niemi, J. V., Manninen, H. E., van  
916 Pinxteren, D., Harrison, R. M., Tuch, T., and Weinhold, K.: Insights into the sources of ultrafine particle numbers at six  
917 European urban sites obtained by investigating COVID-19 lockdowns, *EGUsphere* [preprint],  
918 <https://doi.org/10.5194/egusphere-2023-3053>, 2024.

919 Rönkkö, T., Kuuluvainen, H., Karjalainen, P., Keskinen, J., Hillamo, R., Niemi, J. V., Pirjola, L., Timonen, H. J., Saarikoski,  
920 S., Saukko, E., Järvinen, A., Silvennoinen, H., Rostedt, A., Olin, M., Yli-Ojanperä, J., Nousiainen, P., Kousa, A., Dal  
921 Maso, M.: Traffic is a major source of atmospheric nanocluster aerosol, *Proc. Natl. Acad. Sci.*, 114, 7549–7554.  
922 <https://doi.org/10.1073/pnas.1700830114>, 2017.

923 Rönkkö, T. and Timonen, H.: Overview of sources and characteristics of nanoparticles in urban traffic-influenced areas, *J.*  
924 *Alzheimer's Dis.*, 72, 15–28, <https://doi.org/10.3233/jad-190170>, 2019.

925 Salma, I. and Németh, Z.: Dynamic and timing properties of new aerosol particle formation and consecutive growth events,  
926 *Atmos. Chem. Phys.*, 19, 5835–5852, <https://doi.org/10.5194/acp-19-5835-2019>, 2019.

927 Salma, I., Maenhaut, W., and Záray, Gy.: Comparative study of elemental mass size distributions in urban atmospheric  
928 aerosol, *J. Aerosol Sci.*, 33, 339–356, [https://doi.org/10.1016/S0021-8502\(01\)00176-8](https://doi.org/10.1016/S0021-8502(01)00176-8), 2002.

929 Salma, I., Maenhaut, W., Chi, X., Ocskay, R., Záray, Gy.: Mass size distribution of particulate matter in the urban  
930 atmosphere, *J. Aerosol Sci.*, 34S1, 693–694, 2003.

931 Salma, I., Borsós, T., Weidinger, T., Aalto, P., Hussein, T., Dal Maso, M., and Kulmala, M.: Production, growth and  
932 properties of ultrafine atmospheric aerosol particles in an urban environment, *Atmos. Chem. Phys.*, 11, 1339–1353,  
933 <https://doi.org/10.5194/acp-11-1339-2011>, 2011.

934 Salma, I., Füre, P., Németh, Z., Farkas, Á., Balásházy, I., Hofmann, W., and Farkas, Á.: Lung burden and deposition distribution  
935 of inhaled atmospheric urban ultrafine particles as the first step in their health risk assessment, *Atmos. Environ.*, 104, 39–  
936 49, <https://doi.org/10.1016/j.atmosenv.2014.12.060>, 2015.

937 Salma, I., Németh, Z., Weidinger, T., Kovács, B., and Kristóf, G.: Measurement, growth types and shrinkage of newly  
938 formed aerosol particles at an urban research platform, *Atmos. Chem. Phys.*, 16, 7837–7851, <https://doi.org/10.5194/acp-16-7837-2016>, 2016a.

939 Salma, I., Németh, Z., Kerminen, V.-M., Aalto, P., Nieminen, T., Weidinger, T., Molnár, Á., Imre, K., and Kulmala, M.:  
940 Regional effect on urban atmospheric nucleation, *Atmos. Chem. Phys.*, 16, 8715–8728, <https://doi.org/10.5194/acp-16-8715-2016>, 2016b.

941 Salma, I., Vörösmarty, M., Gyöngyösi, A. Z., Thén, W., and Weidinger, T.: What can we learn about urban air quality with  
942 regard to the first outbreak of the COVID-19 pandemic? A case study from central Europe, *Atmos. Chem. Phys.*, 20,  
943 15725–15742, <https://doi.org/10.5194/acp-20-15725-2020>, 2020.

944 Salma, I., Thén, W., Aalto, P., Kerminen, V.-M., Kern, A., Barcza, Z., Petäjä, T., and Kulmala, M.: Influence of vegetation  
945 on occurrence and time distributions of regional new aerosol particle formation and growth, *Atmos. Chem. Phys.*, 21,  
946 2861–2880, <https://doi.org/10.5194/acp-21-2861-2021>, 2021.

947 Shi, J. P. and Harrison, R. M.: Investigation of ultrafine particle formation during diesel exhaust dilution, *Environ. Sci.*  
948 *Technol.* 33, 3730–3736. <https://doi.org/10.1021/es981187l>, 1999.



951 Squizzato, S., Masiol, M., Emami, F., Chalupa, D., Utell, M., Rich, D., and Hopke, P.: Long-term changes of source  
952 apportioned particle number concentrations in a metropolitan area of the northeastern United States, *Atmosphere*, 10, 27,  
953 <https://doi.org/10.3390/atmos10010027>, 2019.

954 Souza, C. R.: The Accord.NET Framework, <http://accord-framework.net> (last access: 10 September 2023), 2014.

955 Teinilä, K., Timonen, H., Aurela, M., Kuula, J., Rönkkö, T., Hellén, H., Loukkola, K., Kousa, A., Niemi, J. V., and  
956 Saarikoski, S.: Characterization of particle sources and comparison of different particle metrics in an urban detached  
957 housing area, Finland, *Atmos. Environ.*, 272, 118939, <https://doi.org/10.1016/j.atmosenv.2022.118939>, 2022.

958 Thén, W. and Salma, I.: Particle number concentration: a case study for air quality monitoring, *Atmosphere*, 13, 570,  
959 <https://doi.org/10.3390/atmos13040570>, 2022.

960 Trechera, P., Garcia-Marlès, M., Liu, X., Reche, C., Pérez, N., Savadkoobi, M., Beddows, D., Salma, I., Vörösmarty, M.,  
961 Casans, A., Casquero-Vera, J. A., Hueglin, C., Marchand, N., Chazeau, B., Gille, G., Kalkavouras, P., Mihalopoulos, N.,  
962 Ondráček, J., Zíkova, N., Niemi, J. V., Manninen, H. E., Green, D. C., Tremper, A. H., Norman, M., Vratolis, S.,  
963 Eleftheriadis, K., Gómez-Moreno, F. J., Alonso-Blanco, E., Gerwig, H., Wiedensohler, A., Weinhold, K., Merkel, M.,  
964 Bastian, S., Petit, J.-E., Favez, O., Crumeyrolle, S., Ferlay, N., Martins Dos Santos, S., Putaud, J.-P., Timonen, H.,  
965 Lampilahti, J., Asbach, C., Wolf, C., Kaminski, H., Altug, H., Hoffmann, B., Rich, D. Q., Pandolfi, M., Harrison, R. M.,  
966 Hopke, P. K., Petäjä, T., Alastuey, A., and Querol, X.: Phenomenology of ultrafine particle concentrations and size  
967 distribution across urban Europe, *Environ. Int.*, 172, 107744, <https://doi.org/10.1016/j.envint.2023.107744>, 2023.

968 Uria-Tellaetxe, I. and Carslaw, D. C.: Conditional bivariate probability function for source identification, *Environ. Modell.*  
969 *Softw.*, 59, 1–9, <https://doi.org/10.1016/j.envsoft.2014.05.002>, 2014.

970 US EPA: Positive matrix factorization model for environmental data analyses, [https://www.epa.gov/air-research/positive](https://www.epa.gov/air-research/positive-matrix-factorization-model-environmental-data-analyses)  
971 [matrix-factorization-model-environmental-data-analyses](https://www.epa.gov/air-research/positive-matrix-factorization-model-environmental-data-analyses) (last access: 10 September 2023), 2014.

972 US EPA: Criteria air pollutants, <https://www.epa.gov/criteria-air-pollutants> (last access: 20 December 2023), 2023.

973 Vu, T. V., Delgado-Saborit, J. M., and Harrison, R. M.: Review: Particle number size distributions from seven major sources  
974 and implications for source apportionment studies, *Atmos. Environ.*, 122, 114–132,  
975 <https://doi.org/10.1016/j.atmosenv.2015.09.027>, 2015.

976 Vratolis, S., Gini, M. I., Bezantakos, S., Stavroulas, I., Kalivitis, N., Kostenidou, E., Louvaris, E., Siakavaras, D., Biskos, G.,  
977 Mihalopoulos, N., Pandis, S. N., Pilinis, C., Papayannis, A., and Eleftheriadis, K.: Particle number size distribution  
978 statistics at city-centre urban background, urban background, and remote stations in Greece during summer, *Atmos.*  
979 *Environ.*, 213, 711–726, <https://doi.org/10.1016/j.atmosenv.2019.05.064>, 2019.

980 Viana, M., Kuhlbusch, T. A. J., Querol, X., Alastuey, A., Harrison, R. M., Hopke, P. K., Winiwarter, W., Vallius, M., Szidat,  
981 S., Prévôt, A. S. H., Hueglin, C., Bloemen, H., Wählin, P., Vecchi, R., Miranda, A. I., Kasper-Giebl, A., Maenhaut, W.,  
982 and Hitzenberger, R.: Source apportionment of particulate matter in Europe: A review of methods and results, *J. Aerosol*  
983 *Sci.*, 39, 827–849, <https://doi.org/10.1016/j.jaerosci.2008.05.007>, 2008.

984 Wiedensohler, A., Birmili, W., Nowak, A., Sonntag, A., Weinhold, K., Merkel, M., Wehner, B., Tuch, T., Pfeifer, S., Fiebig,  
985 M., Fjåraa, A. M., Asmi, E., Sellegri, K., Depuy, R., Venzac, H., Villani, P., Laj, P., Aalto, P., Ogren, J. A., Swietlicki,  
986 E., Williams, P., Roldin, P., Quincey, P., Hüglin, C., Fierz-Schmidhauser, R., Gysel, M., Weingartner, E., Riccobono, F.,  
987 Santos, S., Gruning, C., Faloon, K., Beddows, D., Harrison, R., Monahan, C., Jennings, S. G., O'Dowd, C. D., Marinoni,  
988 A., Horn, H.-G., Keck, L., Jiang, J., Scheckman, J., McMurry, P. H., Deng, Z., Zhao, C. S., Moerman, M., Henzing, B.,  
989 de Leeuw, G., Lösschau, G., and Bastian, S.: Mobility particle size spectrometers: harmonization of technical standards  
990 and data structure to facilitate high quality long-term observations of atmospheric particle number size distributions,  
991 *Atmos. Meas. Tech.*, 5, 657–685, <https://doi.org/10.5194/amt-5-657-2012>, 2012.

992 Wang, K., Nakao, S., Thimmaiah, D., and Hopke, P. K.: Emissions from in-use residential wood pellet boilers and potential  
993 emissions savings using thermal storage, *Sci. Total Environ.*, 676, 564–576,  
994 <https://doi.org/10.1016/j.scitotenv.2019.04.325>, 2019.

995 Wang, M., Hopke, P. K., Masiol, M., Thurston, S. W., Cameron, S., Ling, F., van Wijngaarden, E., Croft, D., Squizzato, S.,  
996 Thevenet-Morrison, K., Chalupa, D., and Rich, D. Q.: Changes in triggering of ST-elevation myocardial infarction by  
997 particulate air pollution in Monroe County, New York over time: a case-crossover study, *Environ. Health.*, 18, 82,  
998 <https://doi.org/10.1186/s12940-019-0521-3>, 2019.

999 WHO Global Air Quality Guidelines: Particulate matter (PM<sub>2.5</sub> and PM<sub>10</sub>), ozone, nitrogen dioxide, sulfur dioxide and  
1000 carbon monoxide, <https://www.ncbi.nlm.nih.gov/books/NBK574594/>, World Health Organization (last access: 10  
1001 September 2023), 2021.

1002 Yoshizumi, K.: Regional size distributions of sulfate and nitrate in the Tokyo metropolitan area in summer, *Atmos. Environ.*,  
1003 20, 763–766, [https://doi.org/10.1016/0004-6981\(86\)90191-5](https://doi.org/10.1016/0004-6981(86)90191-5), 1986.

- 1004 Zhang, Y., Zhang, Q., Yao, Z., and Li, H.: Particle size and mixing state of freshly emitted black carbon from different  
1005 combustion sources in China, *Environ. Sci. Technol.*, 54, 7766–7774, <https://doi.org/10.1021/acs.est.9b07373>, 2020.
- 1006 Zhou, L., Kim, E., Hopke, P. K., Stanier, C., and Pandis, S. N.: Advanced factor analysis on Pittsburgh particle size-  
1007 distribution data, *Aerosol Sci. Technol.*, 38, 118–132, <https://doi.org/10.1080/02786820390229589>, 2004.